

## Estimation of reflection coefficients from zero-offset field data

Borge Arntsen\* and Bjorn Ursin†

### ABSTRACT

The classical one-dimensional (1-D) inverse problem consists of estimating reflection coefficients from surface seismic data using the 1-D wave equation. Several authors have found stable solutions to this problem using least-squares model-fitting methods. We show that the application of these plane-wave solutions to seismic data generated with a point source can lead to errors in estimating reflection coefficients. This difficulty is avoided by using a least-squares model fitting scheme describing vertically traveling waves originating from a point source. It is shown that this method is roughly equivalent to deterministic deconvolution with built-in multiple removal and compensation for spherical spreading. A true zero-offset field data set from a specially designed seismic experiment is then used as input to estimate reflection coefficients. Stacking velocities from a conventional seismic survey were used to estimate spherical spreading. The resulting reflection coefficients are shown to correlate well with an available well log.

### INTRODUCTION

The classical one-dimensional (1-D) inverse problem consists of estimating reflection coefficients from surface seismic data using the 1-D wave equation. The problem has been treated by many authors. Reviews of these works are found in Bube and Burridge (1983) and Newton (1981). The classical solution was given by Kunetz (1963). This solution is however known to be unstable in the presence of noise, as shown by Bamberger et al. (1982), who gave a stable method based on least-squares model fitting. This work also contained inversion results using real prestack surface seismic data. Mace and Lailly (1986) showed how the same method

could be applied to a vertical seismic profile (VSP). An example of inverting a real VSP was also given. Grivelet (1985) applied a similar method to a real VSP data set. Gersztenkorn et al. (1986) used a least-squares method and a reweighted least-squares method to solve the 1-D inverse problem; However, only synthetic data examples were given. Recently, Landro and Ursin (1988) used a least-squares detection scheme to estimate reflection coefficients from zero-offset field data. In one spatial dimension, only plane waves propagating along one axis can be described, not spherical waves originating from a point source. To use methods based on the 1-D wave equation, some kind of scaling of the input data must be performed. As shown by Ursin and Bertheussen (1986) and Ursin and Arntsen (1985), this leads to incorrect amplitudes of the multiple reflections, which leads to incorrect estimates of the reflection coefficients. We avoid this difficulty by considering the inverse problem of predicting reflection coefficients from vertically traveling spherical waves in a 1-D horizontally layered medium, taking spherical spreading properly into account.

A conventional marine seismic experiment is far from a true zero-offset experiment, leading to difficulties when a 1-D wave equation is used to describe such an experiment (Ursin and Bertheussen, 1986). To avoid this, a special zero-offset marine seismic experiment was performed in an area that is known to be approximately horizontally stratified.

We approach the solution of the inverse problem with a least-squares, model-fitting scheme. The forward modeling is based on ray theory and is able to simulate a true zero-offset experiment in a horizontally layered medium. The effects of three-dimensional (3-D) spherical spreading are included, as well as first-order multiple reflections related to the free surface. The time used to compute the forward model increases exponentially with the number of reflections (Arntsen, 1988), so for practical reasons it was chosen to include all surface multiples with three reflections (also counting the surface reflection). Since the amplitudes of

Presented at the 61st Ann. Internat. Mtg., Society of Exploration Geophysicists. Manuscript received by the Editor March 9, 1992; revised manuscript received April 15, 1993.

\*Statoil Research Centre, Posttuttak, 7004 Trondheim, Norway.

†Division of Petroleum Engineering and Applied Geophysics, The Norwegian Institute of Technology, N-7034 Trondheim-NTH, Norway.

© 1993 Society of Exploration Geophysicists. All rights reserved.

multiples decrease with the number of reflections (Arntsen, 1988), this should be a reasonable approximation. However, even if higher order multiples are not detectable as single events, they could affect the shape of the seismic signal. In our formulation this would show up as noise in the inversion process.

We show that the resulting inverse scheme is equivalent to iterative inverse Wiener filtering with respect to the known source pulse and with built-in removal of the first-order free surface multiples and compensation for spherical spreading and transmission losses. The inverse scheme can be straightforwardly generalized to the two-dimensional (2-D) case, by using 2-D forward modeling based on dynamic ray tracing. Mora (1987) gives an example of such a scheme, but wave velocities and densities are estimated instead of reflection coefficients. Also, only primary reflections are included in the forward model.

The first section describes the forward ray modeling algorithm that is used. The forward modeling is very efficient and allows easy inclusion of spherical spreading. The second section gives the details of the inversion algorithm. The algorithm minimizes the difference between synthetic data generated by ray modeling and measured field data. The third section examines the relation between least-squares inversion and deterministic deconvolution. The effects of scaling data obtained with a point source to mimic plane wave data is discussed in the fourth section, while the fifth section describes acquisition of the zero-offset field data and the application of the inverse algorithm to this data set.

## MODELING

A medium consisting of a stack of  $L$  elastic plane layers is considered. The stack is bounded by half-spaces at the top and bottom, which are numbered 0 and  $L + 1$ , respectively. Layer  $k$  is above interface  $k$ . Each layer is characterized by the thickness  $D_k$ , P-wave velocity  $c_k$ , and density  $\rho_k$ . The receiver and source are located in the first layer. It is assumed that the pressure at the source position is given. As shown by Ursin and Arntsen (1985), the elastic wave-equation can be approximately solved by a ray series expansion. The solution is valid for waves with the direction of propagation along the vertical axis.

The pressure  $p$  at the receiver caused by a single ray can be expressed in the following form:

$$p(t) = AFg(t - \tau). \quad (1)$$

$A$  is a factor containing products of reflection and transmission coefficients, while  $F$  accounts for the spherical spreading. Function  $g$  is related to the wavefield at the source, while  $\tau$  is the traveltime and  $t$  denotes the time.

The source function  $g$  is a sum of contributions from waves reflected at the surface and a directly transmitted wave:

$$g(t) = g_0(t + \Delta\tau_r + \Delta\tau_s) + r_0g_0(t - \Delta\tau_r + \Delta\tau_s) + r_0g_0(t - \Delta\tau_s + \Delta\tau_r) + r_0^2g_0(t - \Delta\tau_r - \Delta\tau_s). \quad (2)$$

Element  $g_0$  is the source pulse, while  $\Delta\tau_s$  and  $\Delta\tau_r$  are the contributions to the traveltime along the path from the top of the first layer to the receiver and source positions, respec-

tively. Element  $r_0$  is the reflection coefficient at the surface. The deghosted source pulse  $g_0$  is assumed to be known. Also in equation (2) it is assumed that the depth of the receiver and source are small compared to the total length of the raypath, making it possible to neglect the difference in spherical spreading between a reflected wave and its ghost reflection from the upper boundary.

The traveltime  $\tau$  is given by:

$$\tau = \sum_{k=1}^L h_k \Delta\tau_k. \quad (3)$$

The sum runs over all the layers traversed by the ray. Element  $h_k$  is the number of times the ray has traversed layer  $k$ . The contribution  $h_k \Delta\tau_k$  to the traveltime from one layer is:

$$h_k \Delta\tau_k = h_k c_k^{-1} D_k. \quad (4)$$

$A$  can be written as

$$A = \prod_n r_n \prod_k q_k^2. \quad (5)$$

The products of the reflection coefficients  $r_n$  run over every interface at which the ray has been reflected, and the products of the transmission coefficients  $q_k$  run over all the interfaces crossed by the ray. The transmission coefficients are defined in terms of the reflection coefficients as:

$$q_k^2 = 1 - r_k^2. \quad (6)$$

The reflection coefficients are given in terms of the density and wave velocity:

$$r_k = \sigma(\rho_{k+1}c_{k+1} - \rho_k c_k) / (\rho_{k+1}c_{k+1} + \rho_k c_k). \quad (7)$$

Here  $\sigma$  is equal to  $+1$  for a downgoing ray and  $-1$  for an upgoing ray. The function  $F$  accounts for spherical spreading and is written

$$F = c_1/n, \quad (8)$$

where

$$n = \sum_{k=1}^L h_k \Delta n_k. \quad (9)$$

The sum runs over all the layers traversed by the ray. The contribution  $h_k \Delta n_k$  to the spherical spreading from one layer is

$$h_k \Delta n_k = h_k c_k D_k = h_k c_k^2 \Delta\tau_k. \quad (10)$$

Equation (9) can also be readily expressed in terms of the root-mean-square (rms) velocity  $V_{rms}$ :

$$n = \tau V_{rms}^2, \quad (11)$$

where

$$V_{rms}^2 = 1/\tau \sum_{k=1}^L h_k c_k^2 \Delta\tau_k. \quad (12)$$

The total pressure at the receiver position consists of an infinite sum of rays. In any practical calculation, a finite set

of rays must be selected. A reasonable selection criterion is the number of times a given ray has been reflected (Arntsen, 1988). The number of rays grows exponentially with the number of reflections, so only a limited number of reflections can be included in practice. In the numerical examples shown in the next sections, we have included primary reflections and surface multiples reflected three times (including the surface reflection). Any of these events will be larger than other multiples for reflection coefficients (except the reflection coefficient at the surface) of the order of one tenth. However, even if higher order multiples are not detectable as single events, they could affect the shape of the seismic signal. In our formulation this would show up as noise in the inversion process.

The total pressure at the receiver position can then be written as the sum of primary reflections  $p^P$  and first-order surface multiples  $p^M$ :

$$p(t) = p^P(t) + p^M(t). \tag{13}$$

The contribution from the primary reflections is

$$p^P(t) = \sum_{k=1}^L A_k F_k g(t - \tau_k). \tag{14}$$

$F_k = c_1 n_k^{-1}$  is the spherical spreading for the primary reflection from layer  $k$ , and  $\tau_k$  is the corresponding traveltime. The amplitude  $A_k$  is given by:

$$A_k = r_k \prod_{\ell=1}^{k-1} q_\ell^2. \tag{15}$$

For first-order surface multiples, the contribution to the total pressure is given by:

$$p^M(t) = \sum_{\ell=1}^L \sum_{m=1}^L A_\ell A_m r_0 F_{\ell m} g(t - \tau_\ell - \tau_m). \tag{16}$$

$F_{\ell m} = c_1 (n_\ell + n_m)^{-1}$  is the spherical spreading for a wave reflected at the surface and at interfaces  $\ell$  and  $m$ .

### INVERSION

The observed (measured) pressure can, in general, be regarded as a (nonlinear) function of the parameters characterizing the layered medium. Using vector notation, the relation between the observed data and the unknown parameters can be written:

$$p^{obs} = \mathbf{p}(\boldsymbol{\theta}). \tag{17}$$

Here the vector  $p^{obs}$  is the observed (measured) data, while the pressure vector  $p$  is the forward model corresponding to equation (1). Both the observed pressure  $p^{obs}$  and the forward model  $p$  are defined by the samples  $p_k^{obs}$  and  $p_k$  at time  $t = (k - 1)\Delta t$ ;

$$p^{obs} = (p_1^{obs}, p_2^{obs}, \dots, p_{N_T}^{obs}), \tag{18}$$

$$\mathbf{p} = (p_1, p_2, \dots, p_{N_T}). \tag{19}$$

Here  $N_T$  is the number of samples. The parameter vector in our case is defined as:

$$\boldsymbol{\theta} = (r_1, \dots, r_L, \tau_1, \dots, \tau_L, n_1, \dots, n_L). \tag{20}$$

Element  $n_k$  is related to the spherical spreading of a ray reflected at interface  $k$  [see equation (14)]. Our aim is to solve equation (17) to obtain an expression for the parameter vector  $\boldsymbol{\theta}$  in terms of the observed pressure vector  $p$ .

In principle, it would be possible to estimate all three sets of parameters, and then calculate density, P-wave velocity, and layer thickness. However, the pressure depends on the traveltimes via the source pulse. In realistic cases this relationship is nonlinear, making it difficult to estimate traveltimes, unless the traveltimes can be approximately obtained from interpretation of the data. Often this is the case, and then corrections to the initial traveltimes can be calculated. This approach is used in inversion of post-stack zero-offset data (van Riel and Berkhout, 1985). The reflection coefficients and the pressure are related in a quasi-linear way, making it easier to obtain their estimates.

In the numerical examples to follow, the spherical spreading factors are assumed to be known and are kept in constant during the inversion process. Instead of estimating the traveltimes, we discretize the medium in layers with equal two-way traveltime. This reduces the number of unknown parameters, and increases the speed of the numerical computations. Then the parameter vector given in equation (20) reduces to:

$$\boldsymbol{\theta} = (r_1, \dots, r_L). \tag{21}$$

Equation (17) is solved with an iterative procedure where the time-integrated squared difference between the measured pressure and the pressure from the forward model is minimized with respect to a set of model parameters. Mathematically the object function given by

$$\int_0^T dt [p^{obs}(t) - p(t)]^2, \tag{22}$$

is minimized with respect to  $\boldsymbol{\theta}$ . We assume that  $q - 1$  iterations have been performed and that the parameter vector  $\boldsymbol{\theta}_{q-1}$  has been estimated. The pressure  $p(0)$  can then be expanded in a Taylor expansion around  $\boldsymbol{\theta}_{q-1}$ :

$$\Delta \mathbf{p}^{(q)} = \mathbf{J}^{(q)} \Delta \boldsymbol{\theta}^{(q)}. \tag{23}$$

Here  $\Delta \mathbf{p}^{(q)} = \mathbf{p}^{obs} - \mathbf{p}(\boldsymbol{\theta}^{(q-1)})$ ,  $\Delta \boldsymbol{\theta}^{(q)} = \boldsymbol{\theta}^{(q)} - \boldsymbol{\theta}^{(q-1)}$  and  $\mathbf{J}^{(q)}$  is the Jacobian matrix whose elements are given by

$$J_{ij}^{(q)} = \partial_{\theta_j} p_i |_{\boldsymbol{\theta} = \boldsymbol{\theta}^{(q-1)}} \tag{24}$$

The notation  $\partial_{\theta_j}$  means  $\partial/\partial\theta_j$ . The Appendix gives the detailed expressions for the Jacobi-matrix in equation (24). The estimate  $\boldsymbol{\theta}^{(q)}$  of the parameter vector in iteration  $q$  is then

$$\boldsymbol{\theta}^{(q)} = \boldsymbol{\theta}^{(q-1)} + \Delta \boldsymbol{\theta}^{(q)}. \tag{25}$$

The parameter update  $\Delta \boldsymbol{\theta}^{(q)}$  is found by solving equation (23) with respect to  $\Delta \boldsymbol{\theta}^{(q)}$ . The least-squares solution to the problem is

$$\Delta \boldsymbol{\theta}^{(q)} = (\mathbf{J}^{(q)T} \mathbf{J}^{(q)} + \lambda \mathbf{I})^{-1} \mathbf{J}^{(q)T} \Delta \mathbf{p}^{(q)}. \tag{26}$$

Here  $\mathbf{I}$  is the identity matrix and  $\lambda$  is a damping factor, chosen just large enough to avoid instabilities of the solution. Several schemes for choosing  $\lambda$  is known, we have used an

adaptive scheme similar to Amundsen and Ursin (1991). The superscript  $T$  denotes transpose.

The approximate solution of equation (17) can now be summarized in the following steps:

- 1) Choose an initial parameter vector  $\theta_0$ . Put  $q = 1$ .
- 2) Compute  $\Delta \mathbf{p}^{(q)}$  and  $\mathbf{J}^{(q)}$  by using equations (23) and (24)
- 3) If the norm of  $\Delta \mathbf{p}^{(1)}$  is less than a prescribed value,  $\theta^{(q-1)}$  is accepted as the solution.
- 4) If the norm of  $\Delta \mathbf{p}^{(q)}$  is not small enough, a new estimate  $\theta^{(q)}$  is computed using equation (25) and (26). Increase  $q$  by one, and repeat steps 2-4.

INVERSION CONTRASTED TO DECONVOLUTION

In this section we will show that each iteration of the inverse scheme outlined in the previous section may be interpreted as a deterministic deconvolution compensating for the effects of the source pulse, followed by spherical spreading correction and compensation for reflection and transmission losses. To show this a Goupillaud medium is considered. Each layer of the medium then has a constant two-way traveltme equal to the time-sampling interval  $\Delta t$  of the data. It is assumed that initially all reflection coefficients are equal to zero. The residual is then equal to  $\Delta \mathbf{p}^{(1)} = \mathbf{p}^{obs}$ . Equation (26) gives the reflection coefficients for the first iteration as:

$$\mathbf{r}^{(1)} = (\mathbf{J}^{(1)T} \mathbf{J}^{(1)} + \lambda \mathbf{I})^{-1} \mathbf{J}^{(1)T} \mathbf{p}^{obs}. \quad (27)$$

The  $ij$ th component of the Hessian matrix  $\mathbf{J}^{(1)T} \mathbf{J}^{(1)}$  is obtained, using the results of the Appendix, as:-

$$(\mathbf{J}^{(1)T} \mathbf{J}^{(1)})_{ij} = \sum_{\ell=1}^{N_T} F_{\ell} g(t_{\ell} - \tau_i) F_{\ell} g(t_{\ell} - \tau_j), \quad (28)$$

where  $t_{\ell} = (\ell - 1)\Delta t$ . The  $i$ th component of the gradient  $\mathbf{J}^{(1)T} \mathbf{p}^{obs}$  is

$$\sum_{\ell=1}^{N_T} \dots \quad (29)$$

Equation (27) is the damped least-squares solution of the linear equation:

$$\mathbf{p}^{obs} = \mathbf{J}^{(1)} \mathbf{r}^{(1)}. \quad (30)$$

In the plane-wave case (i.e., the spherical spreading  $F$  is put equal to one) it is seen from the Appendix that the Jacobian matrix  $\mathbf{J}^{(1)}$  is given by

$$(\mathbf{J}^{(1)})_{ij} = g(t_i - \tau_j)_1 \quad (31)$$

Then equation (30) is equal to the 1-D convolutional model, and equation (27) reduces to the equivalent of the well-known system of normal equations to be solved for the least-squares, zero-delay inverse filtering of the data with

other words, the matrix operator  $(\mathbf{J}^{(1)T} \mathbf{J}^{(1)} + \lambda \mathbf{I})^{-1} \mathbf{J}^{(1)T}$  is a deconvolution operator transforming the data vector  $\mathbf{p}^{obs}$  into the reflection coefficient vector  $\mathbf{r}^{(1)}$ . In the spherical wave case [i.e.,  $F_p$  is given by equation 8)] the Jacobian matrix is equal to:

$$(\mathbf{J}^{(1)})_{ij} = F_i g(t_i - \tau_j). \quad (32)$$

Equation (30) is no longer a convolutional model, and equation (27) must now be interpreted as least-squares inverse filtering with respect to the source pulse  $g(t)$ , with built-in compensation for spherical spreading.

In Figures 2 and 3 the first iteration of the inversion algorithm is illustrated. Here spherical wave propagation is assumed. A simple model, shown in Figure 1, consisting of a single reflector produces data as shown in the upper trace of Figure 2. The first event is the primary reflection and the second event is the first surface multiple reflection. The upper trace of Figure 3 contains the estimated reflection coefficients after the first iteration. Since the initial model was homogeneous (all reflection coefficients equal to zero), the surface multiple is interpreted as a primary reflection. The estimated reflection coefficients are seen to be obtained by spiking deconvolution of the input data. Since the deconvolution also removes the spherical spreading in a proper way, the result is different from a conventional deconvolution.

The second trace in Figure 2 is the difference between the input data in the upper trace and the synthetic data generated from the estimated model in the top trace of Figure 3.

In the second and subsequent iterations the residual is the difference between the input and data and the synthetic data generated in the previous iteration.  $\Delta \mathbf{p}^{(q)} = \mathbf{p}^{obs} - \mathbf{p}^{(q)}$ ,  $q = (2, 3 \dots)$ . The reflection coefficients are obtained as:

$$\mathbf{r}^{(q)} = \mathbf{r}^{(q-1)} + (\mathbf{J}^{(q)T} \mathbf{J}^{(q)} + \lambda \mathbf{I})^{-1} \mathbf{J}^{(q)T} \Delta \mathbf{p}^{(q)}, \quad (33)$$

with the Hessian matrix  $\mathbf{J}^{(q)T} \mathbf{J}^{(q)}$  obtained from the expressions in the Appendix as: -

$$(\mathbf{J}^{(q)T} \mathbf{J}^{(q)})_{ij} = \sum_{k=1}^L \left[ A_i r_i^{-1} F_i g(t_k - \tau_i) + 2r_i^{-1} \sum_{\ell=1}^L r_0 A_i A_{\ell} F_{\ell} g(t_k - \tau_{\ell} - \tau_i) \right]$$

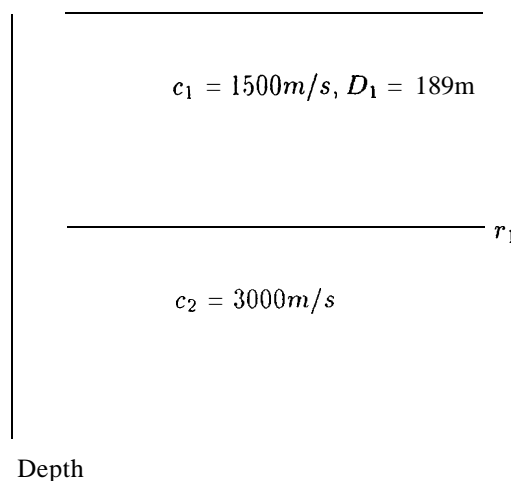


FIG. 1. Model used for the synthetic data example shown in Figures 2 and 3.

$$\begin{aligned}
 & \left. + a_i(t_k) + b_i(t_k) \right] \\
 & \times \left[ A_j r_j^{-1} F_j g(t_k - \tau_j) + 2r_j^{-1} \sum_{\ell=1}^L r_0 A_j A_\ell F_{\ell j} g(t_k - \tau_\ell - \tau_j) \right. \\
 & \left. + a_j(t_k) + b_j(t_k) \right]. \tag{34}
 \end{aligned}$$

The functions  $a_i(t_\ell)$  and  $b_i(t_\ell)$  arise from differentiation of the transmission coefficients, and the detailed expressions for these are given in the Appendix.

The gradient  $\mathbf{J}^{(q)T} \Delta \mathbf{p}^{(q)}$  is now:

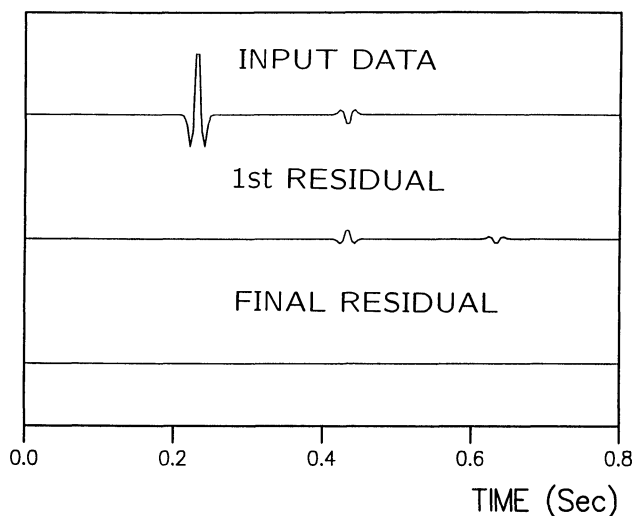


FIG. 2. Input data and residuals for synthetic data example using the model shown in Figure 1.

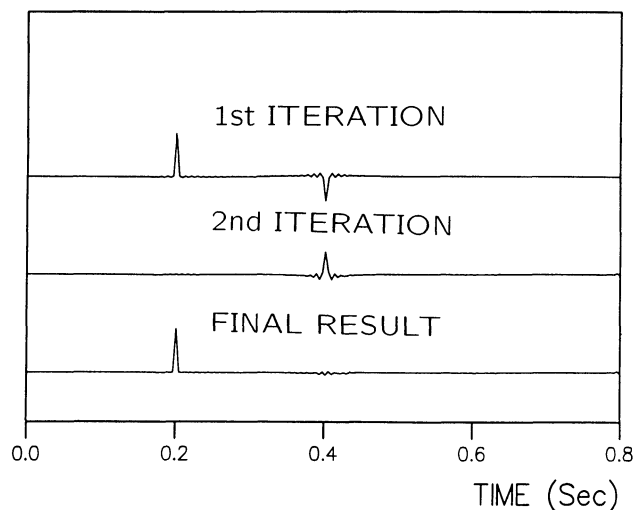


FIG. 3. Estimated reflection coefficients for synthetic data example using the data in Figure 2.

$$\begin{aligned}
 (\mathbf{J}^{(q)T} \Delta \mathbf{p}^{(q)})_i = & \sum_{k=1}^L \left[ A_i r_i^{-1} F_i g(t_k - \tau_i) \right. \\
 & + 2r_i^{-1} \sum_{\ell=1}^L r_0 A_i A_\ell F_{\ell i} g(t_k - \tau_\ell - \tau_i) \\
 & \left. + a_i(t_k) + b_i(t_k) \right] \tag{35}
 \end{aligned}$$

For easier interpretation, transmission effects are for the moment neglected and we consider only plane waves. Then equations (34) and (35) are simplified to:

$$\begin{aligned}
 (\mathbf{J}^{(q)T} \mathbf{J}^{(q)})_{ij} = & \sum_{k=1}^L \left[ g(t_k - \tau_i) + 2 \sum_{\ell=1}^L r_0 r_\ell g(t_k - \tau_\ell - \tau_i) \right] \\
 & \times \left[ g(t_k - \tau_j) + 2 \sum_{\ell=1}^L r_0 r_\ell g(t_k - \tau_\ell - \tau_j) \right], \tag{36}
 \end{aligned}$$

$$(\mathbf{J}^{(q)T} \Delta \mathbf{p}^{(q)})_i = \sum_{\ell=1}^L g(t_\ell - \tau_i) \Delta p^{(k)}(t_\ell). \tag{37}$$

Equations (36), (37), and (33) are the equations to be solved for the least-squares, zero-delay inverse filtering of the data with respect to the known “source pulse”  $g(t) + \sum_{\ell} r_0 r_\ell g(t - \tau_\ell)$ . The second term in the “source pulse” is caused by multiples reflected at the surface. The inverse operator matrix  $(\mathbf{J}^{(q)T} \mathbf{J}^{(q)} + \mathbf{X}\mathbf{I})^{-1} \mathbf{J}^{(q)T}$  not only deconvolves with respect to the source pulse  $g(t)$ , but it also removes multiples explained by the present forward model.

In the more general case where spherical spreading and transmission effects are taken into account, equations (33), (34), and (35) must be solved for the least-squares, temporal inverse filtering of the data with respect to the “source pulse” and least-squares spatial inverse filtering with respect to the spherical spreading. In all of the numerical examples shown, this more general approach is used, so no plane-wave assumptions are introduced.

The second iteration of the inversion algorithm is illustrated in Figures 2 and 3. The second trace from the top in Figure 2 is the input residual  $[\Delta \mathbf{p}^{(2)}]$  to the second iteration of the synthetic example described above. The second trace from the top in Figure 3 is the estimated update  $[\Delta \mathbf{r}^{(2)}]$  of the reflection coefficients. The residual has been deconvolved and the surface multiple in the residual has been removed. The bottom trace of Figure 3 is the sum of the top and middle traces and is the resulting model after two iterations. The surface multiple of the top trace of Figure 2 has now been completely removed. The bottom trace of Figure 2 shows the difference between the input data in the top trace and the synthetic data generated from the model in the bottom trace of Figure 3. As is seen, the inversion scheme converges after two iterations.

In summary, equations (33), (34), and (35) define a time-variant deconvolution operator that deconvolves with respect to the source pulse and surface reverberations and compen-

sates for spherical spreading and transmission effects. Each iteration of the inverse scheme can then be interpreted as subtraction of the data generated by the forward model from the observed data, followed by inverse filtering of the residual with respect to the source pulse, spherical spreading, and multiples explained by the forward model.

PLANE VERSUS SPHERICAL WAVE PROPAGATION

Since point-like sources are commonly used in seismic data acquisition, 1-D plane-wave inverse methods must rely on some kind of scaling of the input data. A common method used in seismic processing is to scale the data with the inverse of the spherical spreading for the primary reflections. Then the observed data  $p^{obs}(t)$  is related to the scaled data  $p^{scaled}(t)$  by the equation

$$p^{scaled}(t) = c_1 V_{rms}^2(t) p^{obs}(t). \tag{38}$$

The scaled data is supposed to mimic data generated by a plane-wave source. The rms velocity  $V_{rms}$  is given by equation (12). Considering one particular primary reflection

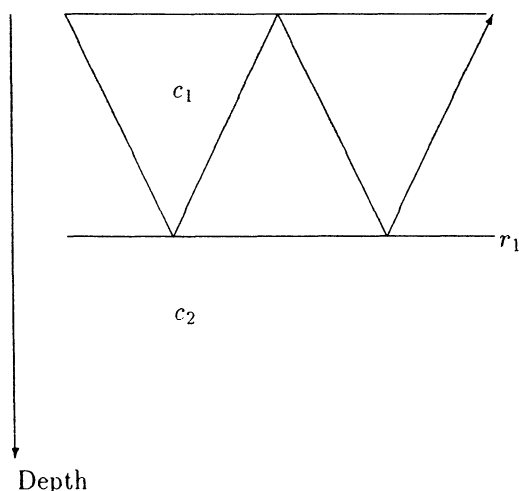


FIG. 4. Model used for the synthetic data example shown in Figures 6 and 7.

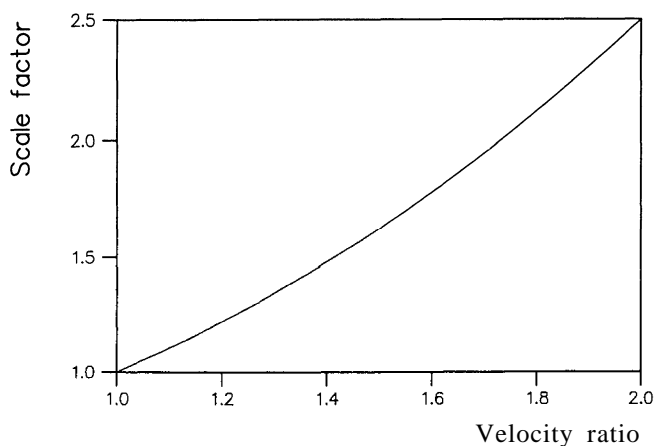


FIG. 5. Spherical spreading correction for a surface multiple.

arriving at time  $t = \tau$  and inserting equation (1) into the right-hand side of equation (38) gives:

$$p^{scaled}(t) = \frac{V_{rms}^2(t)}{V_{rms}^2(\tau)} Ag(t - \tau). \tag{39}$$

The rms-velocity  $V_{rms}^2(t)$  is the rms-velocity calculated along the raypath of a primary reflection arriving at time  $t$ . Ideally, the scaling factor  $V_{rms}^2(t)/V_{rms}^2(\tau)$  should be equal to one for  $t \geq \tau$ , since the plane-wave solution is  $Ag(t - \tau)$ . When  $V_{rms}^2(t \geq \tau)$  is different from  $V_{rms}^2(\tau)$ , errors are made. If a primary reflection arrives at time  $t = \tau$ , then at time  $t = \tau + \Delta t$  the ratio  $V_{rms}^2(\tau + \Delta t)/V_{rms}^2(\tau)$  is larger than one. If  $\Delta t$  is smaller than the pulse duration, then at least the tail of the source pulse is distorted.

The amplitude of multiple reflections are also distorted since the raypaths for primary reflections and multiple reflections are different, leading to different  $V_{rms}$  velocities. It is easy to see this effect using the raypath and the two-layer model shown in Figure 4. The velocity in the upper layer is  $c_1$ , while the velocity in the lower layer is  $c_2$ . The shown surface multiple arrives at time  $t = 2\tau$ . Computing the rms velocity along the raypath of the multiple and inserting this in the denominator of equation (39) gives at time  $t = 2\tau$ :

$$p^{scaled}(t = 2\tau) = \frac{1}{2} \left[ 1 + \left( \frac{c_2}{c_1} \right)^2 \right] Ag(0). \tag{40}$$

The scale factor  $1/2[1 + (c_2/c_1)^2]$  is plotted in Figure 5 as a function of the ratio of the velocity  $c_1$  in the upper layer and the velocity  $c_2$  in the lower layer. It can be seen that the amplitude of the multiple is overestimated even for moderate values of the ratio between the velocity in the upper and lower layers. For inversion, it is important that amplitudes are preserved, since one important aspect of inversion is to extract amplitude information from the input data. Scaling the data as in equation (38) could give incorrect estimates.

In Figure 6 a simple example of the effects of scaling on synthetic data is shown. The top trace shows synthetic data

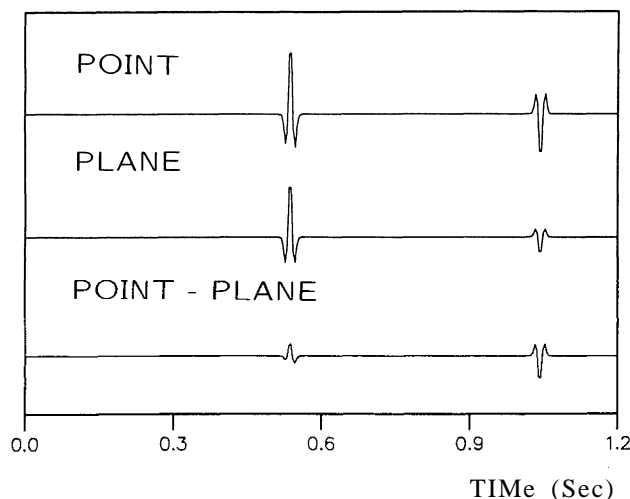


FIG. 6. Synthetic data using the model shown in Figure 4.

generated using the simple two-layer model shown in Figure 4. The data were generated with a point source and have been scaled with the inverse of the spherical spreading for the primary reflection, as given in equation (38). The velocity in the first layer of the model used to generate the data is 1500 m/s while the velocity in the second layer is 3000 m/s. The reflection coefficient at the interface has a value of 0.3. The second trace from the top in Figure 6 shows synthetic data generated from the same model as the point source data, but with a 1-D plane-wave method. The scaled point-source data in the top trace should be equal ideally to the plane-wave data in the second trace. The difference between the two traces is shown in the bottom trace and reflects the errors in the scaling procedure. We see that the amplitude of the primary reflection is incorrect, and that the amplitude of the multiple reflection is two and a half times its correct value, as predicted by equation (40).

The scaled point-source data has been used to estimate the reflection coefficient of the model, using the inverse method described in the previous section but with all spherical spreading factors set equal to one. The top trace of Figure 7 shows the resulting reflection coefficients, while the second trace shows the estimated reflection coefficient using the unscaled point source data and taking the spherical spreading properly into account. The second trace is very close to the exact model. The result shown in the top trace using the scaled point-source data is incorrect, since the amplitude of the estimated reflection coefficient is larger than it should be, and the effect of the multiple reflection has not been removed.

In most cases, errors will not be as large as this example, since the velocity contrast would be smaller than in the chosen example, and hence the difference between the spherical spreading for the primary reflection and the multiple reflection is smaller. Figure 8 shows the result of inverting a real zero-offset trace. The data acquisition will be described in the next section, but the result of applying a plane-wave inversion algorithm to point-source data scaled with the inverse of the spherical spreading for the primary

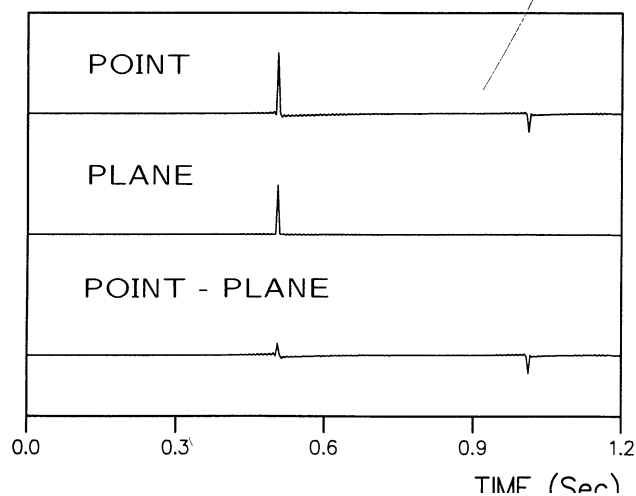


FIG. 7. Estimated reflection coefficients for plane-wave and spherical-wave inverse algorithms using the data shown in Figure 6.

reflections is shown on the leftmost trace. The middle trace is the reflection coefficients resulting from inverting data generated with a point source using the algorithm described in the previous sections. The rightmost trace is the difference between the two other traces. The overall difference is of the order of 10–15 percent, and is caused by the errors made in the scaling of the point-source data. The largest error appears at the earliest times. The spherical spreading was computed from the rms velocities obtained from velocity analysis of conventional seismic data shot in a survey along exactly the same line as the zero-offset data. The rms velocity as a function of travelttime is shown in Figure 9.

#### ZERO-OFFSET FIELD DATA

We wanted to run a more realistic test of the zero-offset inversion than the synthetic data sets would allow. Conventional seismic data is far from zero-offset, and using such data would violate the basic assumptions in the forward modeling. Another major problem was that the wavefield close to the source had to be measured precisely. This is hardly the case in most conventional seismic surveys. To solve these problems, a zero-offset experiment was conducted.

Figure 10 shows the geometry of the zero-offset experiment. The source was a single air gun with a chamber

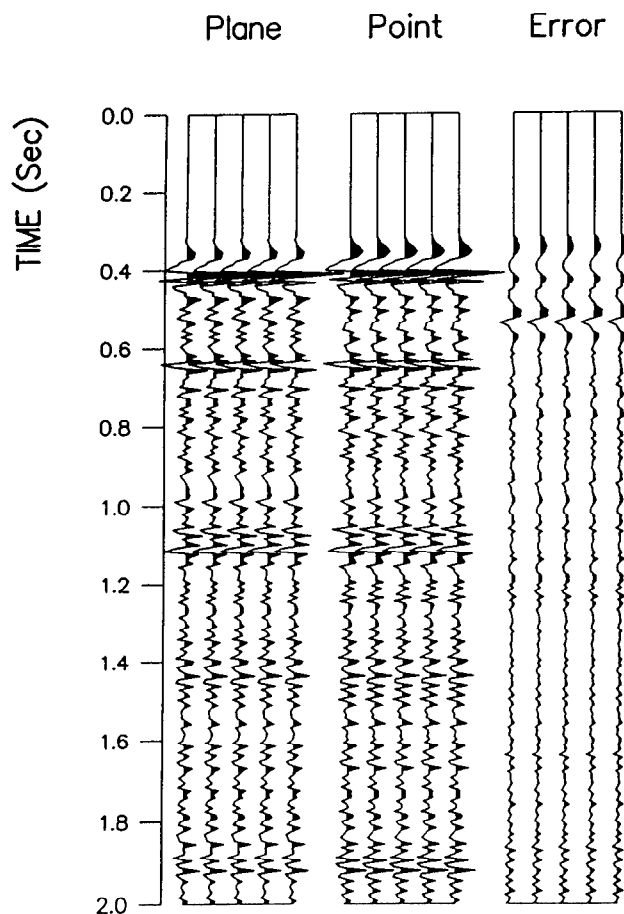


FIG. 8. Estimated reflection coefficients for plane-wave and spherical-wave inverse algorithms using real data.

volume of 9.5 L, while the receiver was a short section (15 m long) of a conventional streamer. In the following we will refer to this as the ministreamer. The hydrophones in the ministreamer had a spacing of 0.7 m. With this setup, a line was shot in the North-Sea over an area that is known to be approximately horizontally stratified. A borehole was located very close to the line, and the sonic and density logs from this borehole were available. The data from a single hydrophone on the streamer section were band-pass filtered and resampled to a sampling interval of 8 ms. The resulting data are shown in Figure 11. A scale factor proportional to time was applied to the data before plotting. The shot interval was 50 m. The source pulse was estimated from the direct arrivals on the ministreamer.

First run

In the first run, only one trace at the borehole position was inverted. No scaling of the data before inversion was applied. The initial model was taken to be reflection coefficients equal to zero for all times. A conventional seismic survey had been performed along a line intersecting the borehole. It was then possible to use rms velocities from a conventional velocity analysis to compute the spherical spreading factor. The inverted reflection coefficients are shown in Figure 12. The norm of the error trace is about 0.07 times the norm of the data trace and is shown in Figure 13, together with the input data. Both have been gained proportional to time for display purposes. The resulting reflection coefficients were obtained after three iterations. Figure 14

shows the relative error between the input data and the synthetic data as a function of iteration number.

Sonic and density logs were available, and these were resampled and then used to compute the reflection coefficients as a function of two-way travelttime. After filtering with a zero-phase band-pass filter, the resulting reflection series was plotted in Figure 12. Comparing the reflection coefficients from the log with the estimated reflection coefficients, the major events correlate reasonably well. The apparent events with large amplitudes at about 1.4 s and 1.6 s on the well-log, are caused by problems with the sonic and density-logs and are not caused by a real reflector. The seafloor is known to contain a double reflector, which is

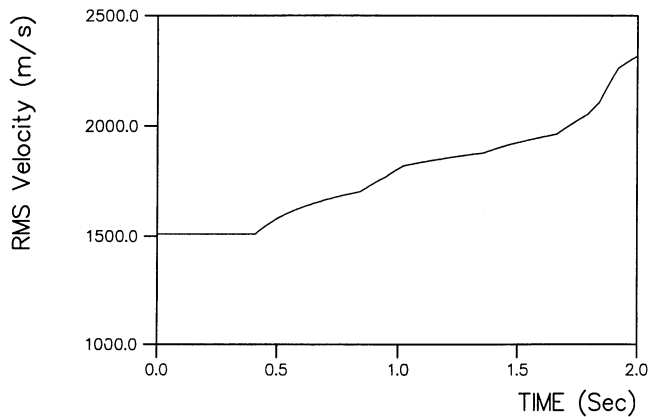


FIG. 9. The rms velocity as a function of travelttime used in the example shown in Figure 8.

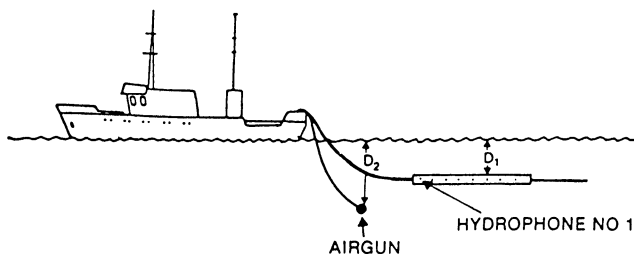


FIG. 10. Geometry of the zero-offset experiment.

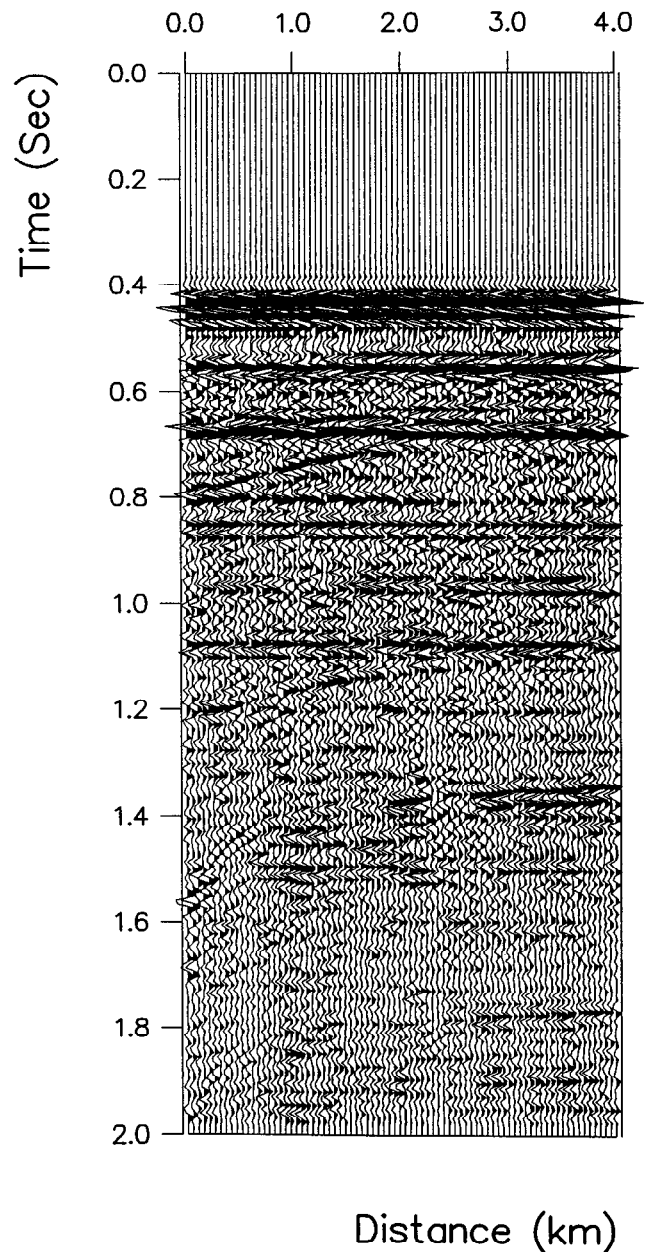


FIG. 11. The zero-offset field data.

evident from Figure 12. Also the sign of the reflection coefficient is positive, as it should be.

Second run

In the second run, eighty traces were inverted. The resulting section of reflection coefficients is shown in Figure 15. The reflection coefficients were only scaled by a constant factor before plotting. The error traces are shown in Figure 16. The error traces are scaled in the same way as the data traces in Figure 11. Comparing the estimated reflection coefficients with the input data, several features can be noted. The long tail of the source signature caused by bubble oscillations has been reduced, and the effects of spherical spreading have, of course, been removed. However, since the source pulse was not precisely estimated, the removal of the tail of the pulse was not perfect and on some traces a substantial residual remains.

CONCLUSIONS

We have given an inverse method for computing reflection coefficients from zero offset field data. Spherical spreading is

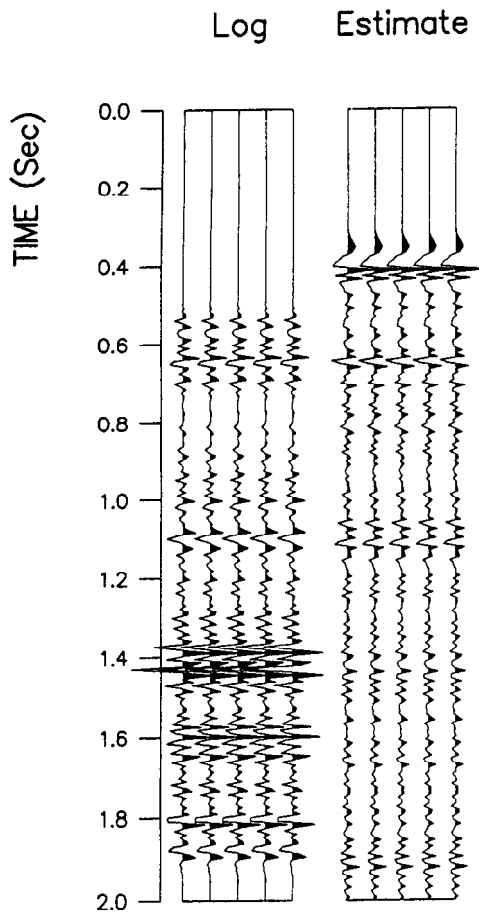


FIG. 12. Estimated reflection coefficients and reflection coefficients computed from a well-log. Both traces are plotted five consecutive times. The well-log is unreliable in the interval below approximately 1.4 s. No log was available above approximately 0.5 s.

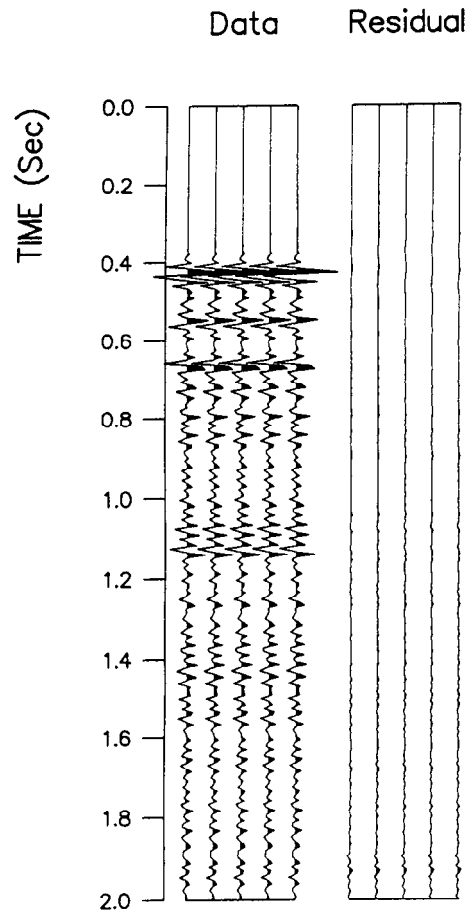


FIG. 13. Data and error trace at the well position. Both traces are plotted five consecutive times.

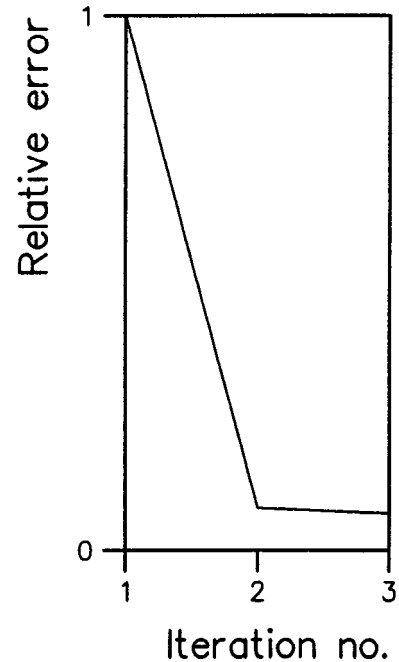


FIG. 14. Relative error between synthetic data and real data as a function of iteration number.

properly taken into account by using rms velocities from a conventional seismic survey. This eliminates the need for any scaling of the input data. It is shown that the least-squares inversion can be interpreted essentially as iterative deterministic deconvolution, with built-in spherical spreading compensation and compensation for transmission effects. Only first-order surface multiples have been included in the inverse scheme. Higher order multiples will be treated as noise, and could degrade the results. It is straightforward to include higher order multiples, but the computational time increases exponentially with the number of layers and the number of reflections. In practice a limited set of multiples must be selected.

A zero offset experiment has been conducted, and the inverse method was used to estimate reflection coefficients from a short marine seismic line. The estimates correlate well with reflection coefficients obtained from well logs. It is, however, clear that a straightforward comparison is not without problems. After all, well log measurements are performed over intervals of the order of 10 cm, which is much less than seismic wavelengths. Since the seismic waves "see" another medium than the well log measurements, one should expect some differences between the estimated reflection coefficients and the reflection coefficients obtained from the well log.

Differences between the estimates and the log that are not accounted for by differences of scale may, in general, be

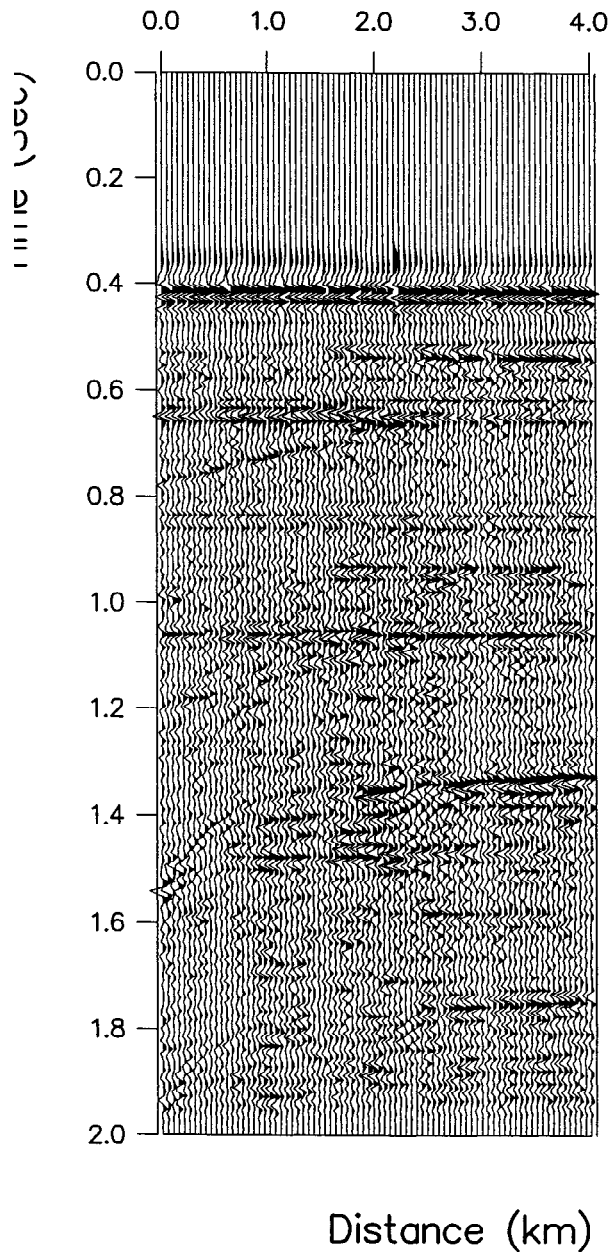


FIG. 15. Estimated reflection coefficients using zero-offset field data.

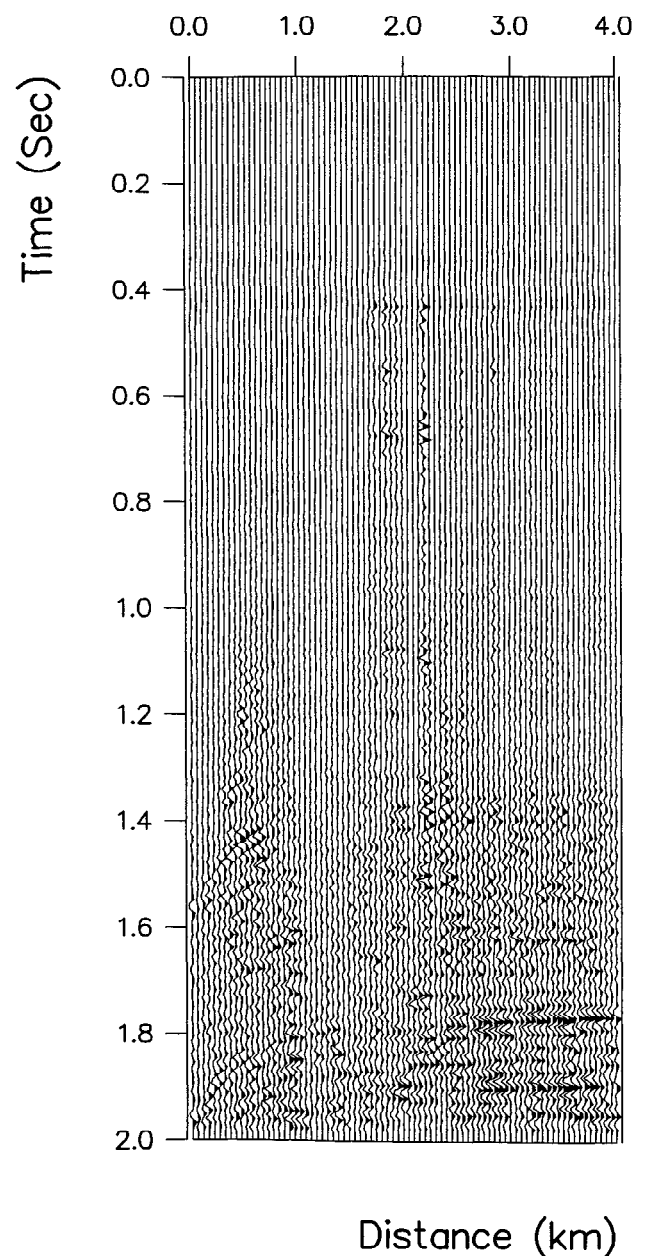


FIG. 16. Zero-offset field data error section.

explained by inaccuracies in the forward model. In the present example, we do not take into account change in bandwidth with time, which will lead to estimates of the reflection coefficients smaller than their actual value. Deviations from horizontal layering would lead to unpredictable errors in the estimates of the reflection coefficients. Errors of this kind should be expected to be present in the estimates of the reflection coefficients in the left part of Figure 15, since deviations from a horizontally stratified medium are evident. Inaccurate measurements of the source pulse would lead to incorrect estimates of the reflection coefficients, and to fully exploit inverse methods, better measurements of the source pulse are very important.

Zero-offset data contain only a small part of the information potentially found in conventional offset data. Ideally, one should use as wide an offset range as possible in any seismic experiment. However, the method we have presented requires much less computer resources than similar methods that handle offset data in a 1-D medium. (Amundsen and Ursin, 1991; Mora, 1987).

It is straightforward to generalize our inverse scheme to the case of a 1-D plane layered medium with 3-D wave propagation. In fact, Mora (1987) proposed such a scheme using ray theoretical forward modeling. Only primary reflections were included in the forward model, and only synthetic data examples were given. Mora's objective was to estimate wave velocities and density, which is a highly nonlinear problem and difficult to solve. Estimating reflection coefficients is a quasi-linear problem and much easier to solve than estimating wave velocities and density. The relation between inversion and migration have been discussed by Tarantola (1984). He found that the first iteration of inversion is closely related to migration. However, a detailed comparison of nonlinear inversion and migration remains to be done, and is left for future research.

#### ACKNOWLEDGMENTS

We wish to thank Martin Landrø who estimated the source signatures and made them available to us and

Svein Vaage who was essential to the design and implementation of the data acquisition of the zero-offset data. W. S. Harlan and three anonymous reviewers provided useful comments. We also wish to thank the crew of R/V Håkon Mosbye.

#### REFERENCES

- Amundsen, L., and Ursin, B., 1991, Frequency-wavenumber inversion of acoustic data: *Geophysics*, 56, 1027-1039.
- Arntsen, B., 1988, Numerical ray generation in the computation of synthetic vertical seismic profiles: *Geophys. Prosp.*, 36, 478-503.
- Bamberger, A., Chavent, G., Hemon, Ch., and Lailly, P., 1982, Inversion of normal incidence seismograms: *Geophysics*, 47, 757-770.
- Bube, P. K., and Burridge, B., 1983, The one-dimensional inverse problem of reflection seismology: *SIAM Review*, 25, 497-559.
- Cardimona, S., 1991, Waveform inversion and digital filter theory: *Geophysics*, 56, 534-536.
- Gersztenkom, A., Bednar, B. J., and Lines, L. R., 1986, Robust iterative inversion for the one-dimensional acoustic wave equation: *Geophysics*, 51, 357-368.
- Grivelet, P., 1985, Inversion of vertical seismic profiles by iterative modelling: *Geophysics*, 50, 924-930.
- Kunetz, G., 1963, Quelques exemples d'analyse de denregistrement sismiques: *Geophys. Prosp.*, 11, 409.
- Landrø, M., and Ursin, B., 1988, Detection of zero-offset seismic reflections: *First Break*, 6, 385-394.
- Mace, D., and Lailly, P., 1986, Solution of the VSP one-dimensional inverse problem: *Geophys. Prosp.*, 34, 1002-1021.
- Mora, P., 1987, Elastic inversion of seismic data for P-wave velocity, S-wave velocity, and density, in Danbom, S. H., and Domenico, S. N., Eds., *Shear-wave exploration: Soc. Expl. Geophys.*, 199-213.
- Newton, R., 1981, Inversion of reflection data for layered media: a review of exact methods: *Geophys. J. Roy. Astr. Soc.*, 65, 191-215.
- Tarantola, A., 1984, Inversion of seismic reflection data in the acoustic approximation: *Geophysics*, 49, 1259-1266.
- Ursin, B., and Arntsen, B., 1985, Computation of zero offset vertical seismic profiles including geometrical spreading and absorption: *Geophys. Prosp.*, 33, 72-96.
- Ursin, B., and Bertheussen, K. A., 1986, Comparison of some inverse methods for wave propagation in layered media: *Proc. of the IEEE*, 74, 389400.
- van Riel, P., and Berkhout, A. J., 1985, Resolution in seismic trace inversion by parameter estimation: *Geophysics*, 50, 144-1455.

## APPENDIX A

## COMPUTATION OF THE JACOBI MATRIX

The main text (equation (24)) gives the Jacobi-matrix as:

$$\mathbf{J}_{ij}^{(q)} = \partial_{\theta_j} p_i(\theta) |_{\theta = \theta_{q-1}}. \quad (\text{A-1})$$

In the following it is assumed that the components of  $\theta$  consist only of reflection coefficients, so that  $\theta_j = r_j$ . If the iteration index  $q$  is omitted, then equation (A-1) simplifies to:

$$\mathbf{J}_{ij} = \partial_{r_j} p_i(r). \quad (\text{A-2})$$

The total pressure field at the receiver is given in the main text as the sum of primary and first-order surface multiples:

$$p(t) = p^P(t) + p^M(t). \quad (\text{A-3})$$

The contribution from the primary reflections is

$$p^P(t) = \sum_{k=1}^L A_k F_k g(t - \tau_k). \quad (\text{A-4})$$

$F_k = c_1 n_k^{-1}$  is the spherical spreading for the primary reflection from layer  $k$ , and  $\tau_k$  is the corresponding travel-time. The amplitude  $A_k$  is given by:

$$A_k = r_k \prod_{\ell=1}^{k-1} q_{\ell}^2. \quad (\text{A-5})$$

For first-order surface multiples, the contribution to the total pressure is given by:

$$p^M(t) = \sum_{\ell=1}^L \sum_{m=1}^L A_{\ell} A_m r_0 F_{\ell m} g(t - \tau_{\ell} - \tau_m). \quad (\text{A-6})$$

$F_{\ell m} = c_1 (n_{\ell} + n_m)^{-1}$  is the spherical spreading for a wave reflected at the surface and at interfaces  $l$  and  $m$

The partial derivatives with respect to reflection coefficients of the total pressure is found by:

$$\partial_{r_j} p(t) = \partial_{r_j} [p^P(t) + p^M(t)]. \quad (\text{A-7})$$

Inserting equations (A-4) and (A-6) into equation (A-7) one gets:

$$\begin{aligned} (\mathbf{J})_{ij} &= \partial_{r_j} p(t_i) \\ &= A_j r_j^{-1} F_j g(t_i - \tau_j) \\ &\quad + 2r_j^{-1} \sum_{\ell=1}^L r_0 A_{\ell} A_{\ell} F_{\ell} g(t_i - \tau_{\ell} - \tau_j) \\ &\quad + a_j(t_i) + b_j(t_i). \end{aligned} \quad (\text{A-8})$$

Here,  $a_j(t_i)$  and  $b_j(t_i)$  are given by:

$$a_j(t_i) = -2r_j(1 - r_j^2)^{-1} \sum_{\ell=1}^{j-1} A_{\ell} F_{\ell} g(t_i - \tau_{\ell}), \quad (\text{A-9})$$

and

$$\begin{aligned} b_j(t_i) &= -4r_j(1 - r_j^2)^{-1} \\ &\quad \times \sum_{\ell=1}^N \sum_{m=1}^{j-1} r_0 A_m A_{\ell} g(t - \tau_{\ell} - \tau_m). \end{aligned} \quad (\text{A-10})$$

Equation (A-7) is valid for  $j \neq 0$  and  $r_0$  is assumed to be known.